ACS APPLIED MATERIALS & INTERFACES

Research Article

www.acsami.org

Oxidation Reaction of Polyether-Based Material and Its Suppression in Lithium Rechargeable Battery Using 4 V Class Cathode, $LiNi_{1/3}Mn_{1/3}Co_{1/3}O_2$

Takeshi Kobayashi,*[,†] Yo Kobayashi,[†] Masato Tabuchi,[§] Kumi Shono,[†] Yasutaka Ohno,[‡] Yuichi Mita,[†] and Hajime Miyashiro[†]

[†]Materials Science Research Laboratory, Central Research Institute of Electric Power Industry, 2-11-1 Iwado Kita, Komae, Tokyo 201-8511, Japan

[§]DAISO CO., 9 Ohtakasu-cyo, Amagasaki, Hyogo 660-0842, Japan

[‡]Electric Power Engineering Systems Co., 2-11-1 Iwado-kita, Komae, Tokyo 201-8511, Japan

Supporting Information

ABSTRACT: The all solid-state lithium battery with polyether-based solid polymer electrolyte (SPE) is regarded as one of next-generation lithium batteries, and has potential for sufficient safety because of the flammable-electrolyte-free system. It has been believed that polyether-based SPE is oxidized at the polymer/electrode interface with 4 V class cathodes. Therefore, it has been used for electric devices such as organic transistor, and lithium battery under 3 V. We estimated decomposition reaction of polyether used as SPE of all solid-state lithium battery. We first identified the decomposed parts of polyether-based SPE and the conservation of most main chain framework, considering the results of SPE analysis after long cycle operations. The oxidation reaction was found to occur slightly at the ether bond in the main chain with the branched side chain. Moreover, we resolved the issue by introducing a self-sacrificing buffer layer at the interface. The introduction of sodium carboxymethyl cellulose (CMC) to the 4 V class cathode surface led to the suppression of SPE decomposition at the interface as a result of the preformation of a buffer layer from CMC, which was confirmed by the irreversible exothermic reaction during the first charge, using electrochemical calorimetry. The attained 1500 cycle operation is 1 order of magnitude longer than those of previously reported polymer systems, and compatible with those of reported commercial liquid systems. The above results indicate to proceed to an intensive research toward the realization of 4 V class "safe" lithium polymer batteries without flammable liquid electrolyte.

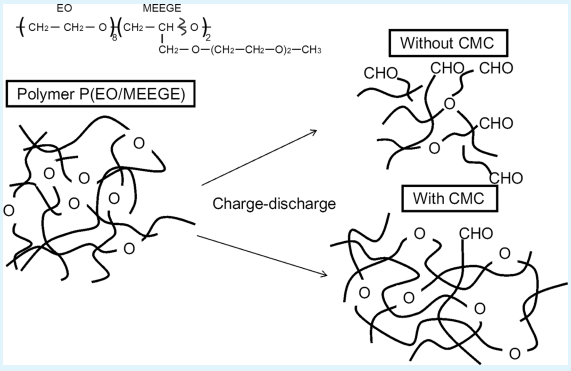

KEYWORDS: *all solid-state lithium polymer battery, solid polymer electrolyte, polyethylene oxide, 4 V-class cathode, carboxymethylcellulose, buffer layer*

1. INTRODUCTION

An electricity storage technique is essential for the effective use of electricity. Rechargeable batteries are expected to be applied as an energy buffer absorbed renewable electric power systems such as photovoltaic and wind power generators.[1,2] A sodium sulfur (NaS) battery has already been used for the storage of electric energy generated from renewable energy sources, and nickel−metal hydride (NiMH) batteries have been extensively used in hybrid cars. Batteries are required to satisfy many properties such as high energy density, high power density, sustainability, and low cost. One of the most promising batteries for satisfying these requirements is a lithium-ion battery. As an increasing number of lithium-ion batteries are being introduced in electric vehicles and for stationary use, improvements in safety are needed to extend their range of utilization. One of the most promising candidates for enhancing safety is the all solid-state lithium battery.[3] This battery has the characteristic that its energy density can be increased by adapting common electrode materials used in liquid electrolyte systems, in the case of using a stacked battery to decrease the weight of the outer packaging.[4] There are two types of solid electrolyte used in all solid-state batteries, one is a solid inorganic electrolyte and the other is a solid polymer electrolyte (SPE). The former has the attractive characteristic of high ionic conductivity of 1×10^{-2} S/cm at room temperature with a wide potential window,[5] but also has low flexibility and low chemical stability in humid environments. On the other hand, the SPE has the advantages of material flexibility and high chemical

Received: August 9, 2013
Accepted: October 21, 2013
Published: October 21, 2013

dx.doi.org/10.1021/am403304j | ACS Appl. Mater. Interfaces 2013, 5, 12387−12393

stability in air and the disadvantage of relatively low ionic conductivity at room temperature.[6] It is necessary to increase the ionic conductivity of SPEs by increasing the temperature. Lithium secondary batteries with SPEs have excellent charge/discharge performance at around 60 °C because their ionic conductivity is reported to be close to 1×10^{-3} S/cm.[7] Thus, if operation at 60 °C is acceptable, all solid-state lithium batteries with SPEs are more suitable for industrial use than those with a solid inorganic electrolyte, from the viewpoint of the safety and flexibility of solid electrolytes.

Despite its attractive advantages, the all solid-state lithium battery with a SPE faces the technical challenge of the need to derive a suitable chemical structure for the polymer. A dried polymer electrolyte such as polyethylene oxide has a poor oxidation reaction at the interface between the electrolyte and the cathode at a high potential of around 4 V.[8] Therefore, SPE batteries with 4 V class cathodes such as $LiCoO_2$, $LiNi_{0.8}Co_{0.2}O_2$, and $LiMn_2O_4$ can be practically used for only a few hundred cycles even in the best case, although SPE batteries with 3 V class cathodes such as $LiFePO_4$, V_2O_5, and MnO_2 shows excellent charge−discharge cycling performances.[9−16] It seems reasonable that the SPEs are degraded by the oxidation reaction at the interface of the electrodes.[8] These results suggest that 3 V class cathodes are suitable for long cycling durability of the batteries using SPEs. Thus, we should enhance the durability of SPEs against high voltages to improve batteries with high-energy-density.

In another approach to use the SPEs, the coating of ceramic materials onto 4 V class cathodes has been carried out to prevent direct contact between the SPE and the cathode.[10,17] The reported batteries have a capacity retention of 60% of the initial capacity under 100 cycles. These results show that coating materials such as Li_3PO_4 and $LiAl_{0.5}Ge_{1.5}(PO_4)_3$ cannot perfectly protect the SPE at the interface from the oxidation of the SPE.

Our approach is a simple and extensively utilizable method of avoiding the degradation of the SPE at the interface between the SPE and the electrode with 4 V class cathode materials for the all solid-state lithium polymer battery with prolonged cycle life. Applying our approach, we have markedly improved the cycling performance of discharge capacity in an all solid-state lithium battery with a 4 V class cathode by introducing sodium carboxymethylcellulose (CMC). The carboxyl group of CMC is considered to be the weak point against the oxidation reaction at high voltages over 4 V. The oxidized compound of CMC has been reported to play a role in protecting the electrolyte from its decomposition.[18] Additionally, the addition of CMC in a 4 V class cathode also led to improved charge−discharge cycling performance with a liquid electrolyte.[19,20]

In this paper, we report the improvement of the long cycle operation using a 4 V class NMC cathode with a CMC coating. In addition, the oxidation mechanism of the SPE after prolonged charge−discharge cycling is discussed from the results of various analyses of the SPE.

2. EXPERIMENTAL SECTION

2.1. Electrode and Cell Preparation. Two different SPEs were used for the all solid-state lithium polymer battery; one is an ionic conducting material that is overcoated on the cathode, and the other is a sheet separating the cathode and the anode as reported previously.[18,21] The former electrolyte, used for the overcoating, was an ether-based polymer (P(EO/MEEGE) = 80/20, Daiso Co., Ltd.) with a high molecular weight (M_w) of about 1.5×10^6. The latter electrolyte was a cross-linked polymer sheet with a thickness of approximately 50 μm made of a different ether-based polymer (P(EO/MEEGE/AGE) = 80/18/2, Daiso Co., Ltd.) with a high M_w of about 2.2×10^6.[18] EO is ethylene oxide, which is the main component of both copolymers, MEEGE is 2-(2-methoxyethoxy) ethyl glycidyl ether, which has a branched-side-chain component, and AGE is allyl glycidyl ether, which has a cross-linkable component. Lithium tetrafluoroborate, ($LiBF_4$) (Kishida Chemical Co., Ltd.) and lithium bis(trifluoromethylsulfonyl) amide, (LiTFSA) (Kishida Chemical Co., Ltd.) were dissolved with each of the polymers. $LiBF_4$ was dissolved in P(EO/MEEGE) with acetonitrile (AN) in the molar ratio of [Li]/[O] = 0.1. AN was added to the SPE composed of $LiBF_4$ and P(EO/MEEGE) to a concentration of 90 wt %. On the other hand, the ratio of [Li]/[O] used with the polymer electrolyte sheet was 0.06. $LiBF_4$ and LiTFSA were used for the polymer sheets, respectively.

$LiNi_{1/3}Mn_{1/3}Co_{1/3}O_2$ (NMC) was used for the cathode active material (AM).[22,23] Morphology of NMC is spherical microparticles with average particle size, ca. 10 μm agglomerated the rod-shaped primary particle (100 nm x 1 μm) and was supplied from material company. The cathode mixture was fabricated with weight ratios of AM/CMC/acethylene black(AB)/vapor-grown carbon fiber (VGCF)/SBR = 91/2/3/3/1 wt % (with CMC) and AM/P(EO/MEEGE)/AB/VGCF/SBR = 91/2/3/3/1 wt % (without CMC) for cathode based polymer battery. On the other hand, the cathode mixture was fabricated with weight ratio of AM/Polyvinylidene fluoride (PVdF)/AB/VGCF = 85/9/3/3 wt % for cathode based liquid battery. Styrene-butadiene rubber (SBR) was used as the binder to prevent cohesion decrease between these electrode materials by the degradation of P(EO/MEEGE). CMC was coated onto the surface of the NMC electrode material and was also used as a binder and a thickening agent. The electrode area was 2 cm^2 (ϕ16 mm). The solvent used for the slurry-based polymer and liquid batteries were aqueous solution and N-methyl pyrolidone (NMP) solution.

The process for fabricating the CMC coating on the NMC electrode is described as follows. First, the NMC powder was introduced to the CMC aqueous solution (with CMC) or the noncross-linkable polymer aqueous solution (without CMC) in the container for comparison. The solutions were stirred until the surface of the NMC powder was soaked by aqueous solution. The process of coating on the NMC powder with CMC or the polymer was thus completed. Second, the conductive materials were added to the solutions, and stirred until the solution became uniform. Finally, the process of preparing the electrode slurries was completed by adding the SBR binder to the solution. The electrode slurries were coated on aluminum foil, and the thickness of the active electrode material was ca. 10 μm. Beforehand, the electrode sheet was dried to remove water by heating in air at 100 °C and subsequently in a vacuum atmosphere at 85 °C overnight. The AN solution containing P(EO/MEEGE) and $LiBF_4$ was dripped onto the electrode sheet, which was then soaked at room temperature to impregnate the SPE solutions into the electrode sheet. After AN was removed by heating in vacuum at 85 °C, the cross-linkable polymer electrolyte sheet was placed on the overcoated electrode to enhance the mechanical properties of the SPE, and the composite was heated at 85 °C. Lithium metal was placed in contact with the other side of the cross-linkable polymer electrolyte sheet, which had an area of 2 cm^2 (ϕ16 mm). P(EO/MEEGE) toluene solution was overcoated onto the lithium metal and dried prior to placing the lithium metal on the SPE sheet to obtain good contact between the SPE and lithium metal. These cells were encapsulated in 2032 coin-type batteries in a dry-argon gas-filled glovebox ([O_2] < 0.2 ppm, [H_2O] < 0.1 ppm, Miwa MFG Co., Ltd.).

2.2. Electrochemical Analysis. The charge−discharge properties of the batteries were characterized using Hokuto HJ-1010 SM8, a multichannel galvanostat, in the voltage range of 4.2−2.7 V at 60 °C. The weight of the active electrode material was ca. 3 mg. We prepared two cells and confirmed that no significant difference in the electrochemical properties was observed between the two batteries during the charge−discharge cycles. The capacity data of the lithium polymer batteries were obtained by charge−discharge under C/8 for 2 cycles and under C/4 for 48 cycles, which values were calculated using

150 mAh/g as the estimated nominal capacity, to accelerate the charge−discharge long cycling time.

Three-electrode cells with the SPE were also fabricated to clarify the electrochemical impedance properties at the working electrode/electrolyte interface using the NMC electrode without the contribution of the counter-Li metal/electrolyte interface. The NMC electrode (ϕ16 mm) was used as a working electrode, and Li metal (ϕ19 mm) was used as the counter electrode. The Li reference electrode was placed close to the working electrode, and on the same side of the polymer electrolyte sheet. The assembled cells were encapsulated in an aluminum laminated pouch in the dry-argon gas-filled glovebox. The ac impedance was measured after every charge in charge/discharge processes using the three-electrode cells in the frequency range between 100 kHz and 50 mHz at the applied voltage of ±10 mV. This measurement was conducted at a temperature of 60 °C.

The heat flow during charge processes was measured using a Calvet-type conduction microcalorimeter (MMC-5111-U Tokyo Riko, Tokyo)[24] to clarify the side reaction in the batteries without and with the CMC.

Three-electrode cells with the SPE were also fabricated to clarify the electrochemical impedance properties at the working electrode/electrolyte interface using the NMC electrode without the contribution of the counter-Li metal/electrolyte interface. The NMC electrode (ϕ16 mm) was used as a working electrode, and Li metal (ϕ19 mm) was used as the counter electrode. The Li reference electrode was placed close to the working electrode, and on the same side of the polymer electrolyte sheet. The assembled cells were encapsulated in an aluminum laminated pouch in the dry-argon gas-filled glovebox. The ac impedance was measured after every charge in charge/discharge processes using the three-electrode cells in the frequency range between 100 kHz and 50 mHz at the applied voltage of ±10 mV. This measurement was conducted at a temperature of 60 °C.

2.3. Ex-post Analysis. The chemical bonding of the noncross-linkable polymer, P(EO/MEEGE) after charge/discharge processes was estimated by FTIR measurement using Thermo Nicolet MAGA-IR 560. The overcoated polymer on the cathode materials was sampled after peeling off the polymer sheet with lithium metal, and then it was mechanically exfoliated from the electrode for FTIR measurement.

The chemical functional group and average molecular weight of P(EO/MEEGE) were estimated by ^{1}H-NMR measurement and gel permeation chromatography (GPC) using JEOL JNM-EX270 NMR spectrometer and (shimadzu, Prominence HPLC system and Showa, Shodex KD column) GPC spectrometer. These samples were prepared for extraction by D_2O and by dimethylformamide (DMF). The measurement temperatures were 80 and 60 °C for the NMR and GPC measurements, respectively. The formation of a low-molecular-weight compound after charge−discharge tests was estimated by gas chromatography using a Shimadzu GC-14B spectrometer with the capillary column, TC-1.

3. RESULTS AND DISCUSSION

3.1. Effect of CMC Coating. Figure 1 shows the charge−discharge curves of NMC with and without a CMC coating. The components of the electrodes were NMC/P(EO/MEEGE)/AB/VGCF/SBR for the cathode without CMC and NMC/CMC/AB/VGCF/SBR for the cathode with CMC. From Figure 1, the NMC cathode with the CMC coating is clearly effective for sustaining the charge−discharge cycling capacity of the SPE. To clarify the role of the CMC in the cathode in more detail, the thermal behavior was simultaneously measured for the above two batteries during charge/discharge. Electrochemical calorimetry can be used to clarify the reversible reactions of the active materials in the electrode during charge/discharge on the basis of the change in thermal behaviors, and to determine the side reaction using the irreversible exothermic profiles of lithium-ion batteries.[24] Figure

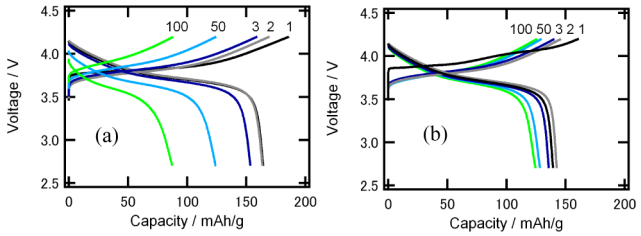

Figure 1. Charge−discharge curves of the all solid-state lithium polymer batteries using the NMC electrode (a) without CMC and (b) with CMC. The charge−discharge curves were plotted for the 1st, 2nd, 3rd, 50th, and 100th cycles.

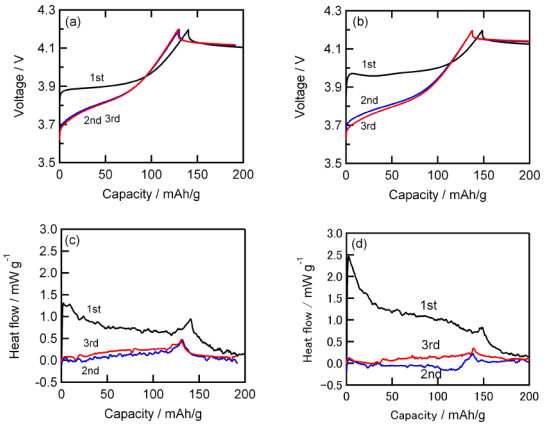

Figure 2. (c, d) Heat flow curves corresponding to (a, b) the charge curves for the first, second, and third cycles in the lithium polymer batteries without CMC and with CMC. Around initial charge process under 20 mAh/g, voltage lump and exthothermic behavior were observed in the battery using CMC compared to that not using CMC.

2 shows the cell voltage and heat flow profiles of the batteries with/without a CMC coating during charging, as obtained by calorimetry. Higher voltage curves were observed in the initial charge cycle only than in the other cycles for both batteries. In detail, there were two differences between the batteries with and without the CMC coating. One is a small bulge in the voltage curve under a capacity of 20 mAh g^{-1} for the battery with CMC in the initial cycle as shown in Figure 2b. The other is a drastic exothermic reaction observed in the battery with CMC in the initial cycle only at capacities of less than 20 mAh g^{-1} (Figure 2d), whereas the corresponding exothermic reaction was small in the battery without CMC (Figure 2c). The bulge in the voltage curve during the first charge was also only observed in the battery with CMC. These anomalous behaviors indicated that the electrochemical reaction of CMC led to the formation of a derivative product of the CMC at a particular voltage. The charge voltage of the cells with aqueous binder was higher than that of the cells with nonaqueous binder at the first cycle. The voltage of the battery at the first cycle was measured to be higher than that from the second cycle because lithium ions were extracted from NMC prepared from the aqueous solution slurries (see the Supporting Information, S1). Figure S1 in the Supporting Information shows the upward shift of the voltage curve of the cell with the aqueous solution compared with that used the nonaqueous solution. In addition, the charge voltage using CMC binder was higher than that upon soaking water on the cathode fabricated with PVdF binder at only first cycle between limited voltage ranges. The CMC may react in these voltage ranges to form the CMC

derivative.Thus, the charge voltage using CMC binder was higher than that upon soaking water on the cathode fabricated with PVdF binder. The product derived from CMC is effective in decreasing the interfacial resistance between the SPE and the NMC. Figure 3 shows impedance spectra of the three-electrode

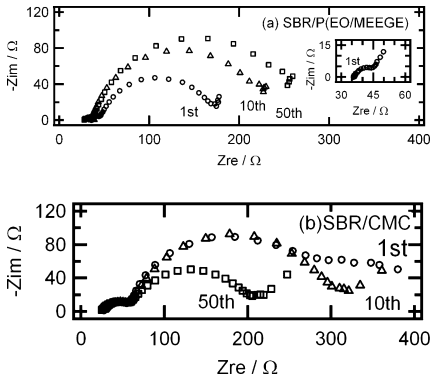

Figure 3. Impedance spectra of the three-electrode cells using the NMC electrode (a) without CMC and (b) with CMC. The curves were plotted for the 1st, 10th, and 50th cycles.

cells using the NMC electrode with/without a CMC coating at the first, 10th, and 50th cycles. Two semicircles were observed for both cells without/with CMC. The semicircle at the low frequency was attributed to the migration of lithium ions at the cathode/electrolyte interface. The enlarged figure of the cell with SBR/P(EO/MEEGE) was inserted into Figure 3a. This attribution of the semicircles in the impedance spectra has been reported by Reale et al.[25] In the cell without CMC, the cathode/electrolyte interfacial resistance increased with repeated charge−discharge cycles. On the other hand, the interfacial resistance decreased for a few cycles and then slowly converged to the ca. 150 Ω after fifty cycles in the battery with CMC. The derivative product of CMC formed during the charge process enhanced the lithium exchange reaction between NMC and the SPE and also led to the suppression of the oxidation reaction of the SPE. Lithium ions could conduct inside the layer of the CMC derivative product according to these results (see the Supporting Information, S2). Figure S2 in the Supporting Information shows the charge−discharge curves of the battery using a SPE sheet coated with CMC. Lithium ions must pass through the CMC layer from the NMC into the lithium metal at the first charge process. The charge curve at the first cycle was observed to be unstable. This phenomenon appears to the formation of the CMC derivative. However, the curve at the second cycle was observed to be stable with same capacity, as that obtained using the normal SPE sheet. This proves the conduction of lithium ions in the CMC derivative layer. The transmutable layer of CMC might act as a buffer layer to protect the SPE and to accelerate the conducting path of lithium ions at the interface. Although we cannot yet identify the chemical structure of the CMC derivative, we consider that it is associated with a carboxyl group of the CMC, and that it has low resistance to the oxidation process. Thus, the CMC derivative may have a similar chemical structure to that of the CMC, but with another group instead of the carboxyl group.

The battery configuration was optimized as described below to obtain the best charge/discharge cycling performance in the all solid-state lithium polymer battery. Normally, lithium dendrites grow slowly in all solid-state lithium polymer batteries compared with in the batteries with a liquid electrolyte. This is because the rigidity of the SPE spatially restricts the growth of lithium dendrites on the interface. However, inhomogeneous contact between the SPE and lithium metal leads to the fast-rapid growth of lithium dendrites owing to the lack of spatial restriction to inhibiting the growth.[26,27] A cross-linkable polymer sheet is relatively solid compared with a non-cross-linkable polymer. Thus, (i) the noncross-linkable polymer, P(EO/MEEGE) was introduced to retain a homogeneous interface on the lithium surface in order to postpone the occurrence of an internal short circuit upon the growth of lithium dendrites. (ii) LiTFSA was substituted for $LiBF_4$ to avoid the corrosive reaction of LiTFSA on the aluminum collector.[28] The optimized battery configuration was Li/P(EO/MEEGE)/P(EO/MEEGE/AGE)/ P(EO/MEEGE)/ NMC with only $LiBF_4$. Figure 4 shows the charge/discharge

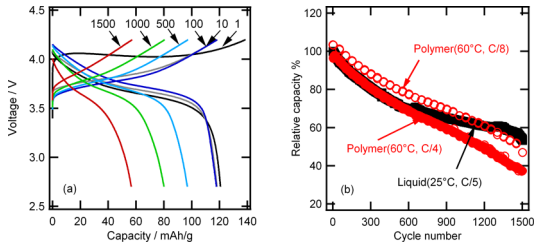

Figure 4. (a) Charge−discharge curves of the lithium polymer battery using the optimized electrode configuration. The curves were plotted for the 1st, 10th, 100th, 500th, 1000th, and 1500th cycles. (b) Discharge capacities plotted versus the number of cycles in the batteries with the SPE and the liquid electrolyte.

curves and cycling curves of the all solid-state lithium polymer battery, as well as the cycling curves of the battery using the liquid electrolyte. In the liquid electrolyte system, PVdF binder was used in the cathode. In contrast, CMC-coated NMC with SBR binder was used in the SPE system. The cycling performance of the battery with the SPE was similar to that of the battery with the liquid electrolyte. The *C*-rate and operation temperature of the battery with the SPE (C/8, 60 °C) were different from as those of the battery with the liquid electrolyte (*C*/5, 25 °C). This was because the initial capacities and the polarization became to be same for the batteries with SPE and the liquid electrolyte. Under the same conditions, the SPE battery is inferior to the liquid electrolyte in terms of the cycling performance. This was because the ionic conductivity of the SPE was lower than that of the liquid electrolyte. However, a high temperature above 60 °C led to the acceleration of NMC degradation.[29] So, if the battery with the liquid electrolyte was operated at 60 °C, the cycling performance would be lower than that of the battery with the SPE. The CMC derivative was responsible for successfully sustaining the cycling capacity. To the best of our knowledge, the achieved charge/discharge cycling performance is the highest cycling performance reported for all solid-state lithium polymer batteries using not only a 4 V class cathode but also other cathodes such as 3 V class cathodes.

3.2. Degradation Mechanism of SPE by Ex-post Analysis. Some chemical analyses were conducted on the polymer in the cathode of the degraded battery to directly elucidate the unknown part of the oxidation decomposition of the polymer and why the capacity decreased after charge−discharge.

Figure 5 shows FT-IR, ^{1}H NMR, and GPC spectra of the polyether in the SPE before and after 1500 charge/discharge

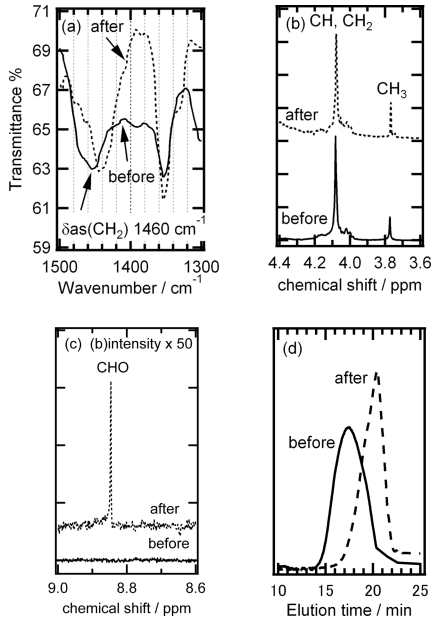

Figure 5. (a) FTIR spectra, (b) high field, and (c) low field regions of ^{1}H NMR spectra, and (d) GPC spectra of the polyether in the SPE before and after 1500 charge−discharge cycles.

cycles. The FTIR sample was prepared by removing the entire SPE from the degraded cathode except for the SPE sheet. FTIR spectra were measured for the SPEs before and after the charge−discharge cycles. A 1456 cm^{-1} signal was attributed to the scissor/deformation mode of asymmetric CH_2 in the polyether chain before charge/discharge.[30] The signal shifted to a lower wavenumber after cycle operations. This indicated that part of the chemical structure of the polyether might change into another chemical structure (see the Supporting Information, S3). Figure S3 shows the FTIR spectra with a wide wavelength range. A 1650 cm^{-1} signal was observed in the polymer after cycle operation. This signal may be attributed the stretching vibration of C═O. Next, the disassembled NMC electrode was washed with D_2O to obtain the polyether from the NMC electrode, and the D_2O solutions dissolved the polymer before and after charge/discharge were subjected to ^{1}H NMR measurement. The insoluble polymer remained on the cathode. The ^{1}H NMR spectra were divided into a high-field region with a chemical shift of 3.4−4.4 ppm and a low-field region with a chemical shift of 8.4−9.0 ppm. In the high-field region, two signals were observed near 4.1 and 3.8 ppm, which were attributed to CH_2, CH, and CH_3 in the polyether. The ratio of the integrals of the two signals was equal to the abundance ratio of CH_2 and CH to CH_3 in the polyether. The ratio was calculated to be 9:1 for the polyethers before and after the charge/discharge process. In the low-field region, a small new signal appeared at around 8.8 ppm after the charge−discharge process. The vertical scale in the graph of the high-field region was 50 times than that for the low-field region. The signal was attributed to an aldehyde group on the basis of a previous report.[31] The FTIR and ^{1}H NMR data also indicated the formation of an aldehyde group from the bonding part of CH_2−O in the polyether. Gas chromatography was performed for the solutions dissolved in polyether that were subjected to the ^{1}H NMR measurements to detect low-molecular-weight compounds in the polyether. However, no such low-molecular-weight compounds were detected in the solutions after repeated charge/discharge. Next, gel permeation chromatography (GPC) was performed to detect the change of the average molecular weight of P(EO/MEEGE). The SPE before and after the charge−discharge process were dissolved into a dimethylformamide (DMF) for GPC measurement. The average molecular weight of P(EO/MEEGE) changed to 1.0 × 10^5 from 1.2 × 10^6 after 1500 cycles (Figure 5d). These results are summarized in Table 1. In addition, GPC was used

Table 1. Summary of Analysis Results of Polyether for Various Numbers of Cycles

no. of cycles	new	500 cycles	1500 cycles
capacity retention	100%	75%	50%
IR	−	no change	δ_{as}(CH2)shift
NMR (highfield) (CH&CH_2):CH_3	9:1	9:1	9:1
NMR (low field)	no signal	no signal	aldehyde group
gas chromatography	undetectable	undetectable	undetectable
gel permeation chromatography	1.2 × 10^6	−	1.0 × 10^5

to estimate the molecular weight of the polymer in the battery, whose configuration was NMC/P(EO/MEEGE)/AB/VGCF/SBR without CMC after about 200 cycles. It was found to be 1.7 × 10^5. The average molecular weight of the polymer in the battery with CMC after 1500 cycles was almost the same as that in the battery without CMC after 200 cycles. The reason why the molecular weight was compared after different numbers of cycles was to unify the amount of side reactions, preventing overestimation of the degradation of the polymer in the battery without CMC. This result means that the CMC self-sacrificial layer coated with NMC plays an important role in suppressing the oxidation of polyether during charging and in prolonging the charge−discharge cycles. However, a slight degradation of the SPE was observed after 1500 cycles, even though the CMC derivative prevents the SPE from undergoing an oxidation reaction. Thus, we discuss which part of the non-cross-linkable polymer decomposes. We attempted to identify the decomposing part of P(EO/MEEGE) after a long numbers of charge−discharge cycles by ^{1}H NMR measurement. Originally, gas chromatography was used to detect compounds with low molecular weights of less than a few hundred, which has a higher sensitivity for detecting compounds with very low concentrations than ^{1}H NMR measurement. We found that no compounds with a low molecular weight were detected by gas chromatography, despite its superior sensitivity to ^{1}H NMR measurement. The lithium salt may be reacted after a large numbers of charge−discharge cycles. If the lithium salt reacts, its reaction will be decomposition, causing its molecular weight to decrease, and its detection by gas chromatography. However, hardly any volatile small molecules were detected by gas chromatography. Finally, an unknown compound with an aldehyde group was detected by ^{1}H NMR measurement after 1500 charge−discharge cycles that did not originate from the side chain of P(EO/MEEGE) and lithium salt. Although influence of the CMC and SBR derivative after charge/discharge operation were also not perfectly ignored against results about the detection of aldehyde group by ^{1}H NMR measurement and the shift of the molecular weight observed in

GPC measurement, their molecular weights were originally under 10 000, and the SBR and CMC derivative should not influence these results. We concluded that the compound originated from the main chain of P(EO/MEEGE). Figure 6

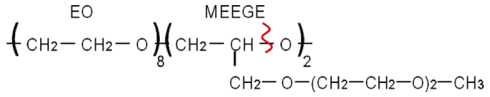

Figure 6. Chemical structure of a P(EO/MEEGE) and the decomposed part of the polyether because of the oxidative reaction.

shows the chemical structure of P(EO/MEEGE) and the oxidation reaction occurring in the main chain with branched polyether in P(EO/MEEGE). The electron density of the main chain, the ether bond of the main chain in MEEGE is more readily attacked by electrons during the charging process than the EO part. This is because the side chain in MEEGE withdraws electrons, causing the electron density of the ether bond to decrease in the MEEGE main chain. This is the first reported evidence that polyether in an SPE is oxidized by prolonged charge−discharge cycling of over 1000 cycles in an all solid-state lithium polymer battery. However, the oxidation reaction of the polyether did not cause sufficient degradation to decrease the cycling capacity of the battery. This is because most of the polymer remained undegraded. The charge−discharge capacity cycling performance of the battery with the SPE was also similar to that of the battery with the liquid electrolyte. This result revealed that the degradation of the cathode material itself was the main factor causing capacity fading of the SPE battery.

4. CONCLUSION

The process we used to coat the $LiNi_{1/3}Mn_{1/3}Co_{1/3}O_2$ (NMC) powder with coating sodium carboxymethyl cellulose (CMC) was simple, and the resulting derivative product played a significant role in improving the charge/discharge cycling performance of the all solid-state lithium polymer battery. The process simply involved mixing the NMC powder and CMC into a slurry. The CMC derivative formed during charging became an effective lithium-ion exchange interface between the NMC electrode and the SPE, and also prevented the SPE from undergoing an oxidation reaction with the NMC electrode. Consequently, the battery exhibited a long cycling performance. The achieved capacity retention after 1500 cycles was 50%, which was unexpectedly similar to that of the battery with a liquid electrolyte. This result means that the previous weak point of the battery with the polyether-based SPE can be overcome by coating the NMC electrode with CMC. The main factor causing the degradation of the battery with the SPE after a large numbers of charge/discharge cycles was found to be not the oxidation reaction of the SPE but the degradation of the cathode at a high temperature, in common with the battery with the liquid electrolyte. An all solid-state lithium polymer battery that can operate for a large numbers of cycles with sufficient safety will help realize a society whose energy requirements are mainly satisfied through a combination of renewable energy sources and rechargeable batteries.

■ ASSOCIATED CONTENT

Ⓢ Supporting Information

Additional charge−discharge curves of a combination of PVdF binder and aqueous solution, and the solid polymer electrolyte coated with CMC film. Additional FTIR spectra with a wide wavelength of the SPE. This material is available free of charge via the Internet at http://pubs.acs.org.

■ AUTHOR INFORMATION

Corresponding Author

*E-mail: kobatake@criepi.denken.or.jp.

Author Contributions

T.K. and Y.K. conceived the battery configuration and the electrochemical experiments as below. Y.O. and K.S fabricated the cathode sheet and the three-electrode cell. T.K. prepared the degraded polymers used in the coin-type battery and carried out the electrochemical experiments. Y.O. and Y.K. carried out the calorimetric experiments. T.K. and M.T. carried out the chemical post analyses. T.K. and Y.K wrote the manuscript. T.K., Y.K., Y.M., and H.M. discussed the results.

Notes

The authors declare no competing financial interest.

■ ABBREVIATIONS

SPE, solid polymer electrolyte
CMC, carboxymethylcellulose
SBR, styrene butadiene rubber
EO, ethylene oxide
MEEGE, 2-(2-methoxyethoxy) ethyl glycidyl ether
AGE, allyl glycidyl ether
LiTFSA, lithium bis(trifluoromethylsulfonil)amide
NMC, $LiNi_{1/3}Mn_{1/3}Co_{1/3}O_2$
AM, active material
AN, acetonitrile
AB, acetylene black
VGCF, vapor grown carbon fiber
DMF, dimethylformamide
FTIR, Fourier transform infrared spectroscopy
GPC, gel permeation chromatography
^{1}H-NMR, proton nuclear magnetic resonance
NMP, N-methyl-2-pyrrolidone

■ REFERENCES

(1) Leadbetter, J.; Swan, L. G. *J. Power Sources* **2012**, *216*, 376−386.
(2) Toledo, O. M.; Oliveira Filho, D.; Diniz, A. S. A. C. *Renewable and Sustainable Energy Reviews* **2010**, *14*, 506−511.
(3) Abraham, K. M. *Electrochim. Acta* **1993**, *38*, 1233−1248.
(4) Munshi, M. Z. A.; Owens, B. B. *Solid State Ionics* **1990**, *38*, 87−94.
(5) Kamaya, N.; Homma, K.; Yamakawa, Y.; Hirayama, M.; Kanno, R.; Yonemura, M.; Kamiyama, T.; Kato, Y.; Hama, S.; Kawamoto, K.; Mitsui, A. *Nat. Mater.* **2011**, *10*, 682−686.
(6) Takeda, Y.; Imanishi, N.; Yamamoto, O. *Electrochemistry* **2009**, *77*, 784−797.
(7) Matoba, Y.; Matsui, S.; Tabuchi, M.; Sakai, T. *J. Power Sources* **2004**, *137*, 284−287.
(8) Li, Q.; Imanishi, N.; Hirano, A.; Takeda, Y.; Yamamoto, O. *J. Power Sources* **2002**, *110*, 38−45.
(9) Li, Q.; Itoh, T.; Imanishi, N.; Hirano, A.; Takeda, Y.; Yamamoto, O. *Solid State Ionics* **2003**, *159*, 97−109.
(10) Seki, S.; Kobayashi, Y.; Miyashiro, H.; Usami, A.; Mita, Y.; Terada, N. *J. Electrochem. Soc.* **2006**, *153*, A1073−A1076.
(11) Kang, Y.; Kim, H. J.; Kim, E.; Oh, B.; Cho, J. H. *J. Power Sources* **2001**, *92*, 255−259.
(12) Nakano, H.; Dokko, K.; Sugaya, J.; Yasukawa, T.; Matsue, T.; Kanamura, K. *Electrochem. Commun.* **2007**, *9*, 2013−2017.
(13) Zhang, D.; Yan, H.; Zhu, Z.; Zhang, H.; Wang, J.; Qilu. *J. Power Sources* **2011**, *196*, 10120−10125.

(14) Hanai, K.; Maruyama, T.; Imanishi, N.; Hirano, A.; Takeda, Y.; Yamamoto, O. *J. Power Sources* **2008**, *178*, 789−794.
(15) Appetecchi, G. B.; Shin, J. H.; Alessandrini, F.; Passerini, S. *J. Power Sources* **2005**, *143*, 236−242.
(16) Xia, Y.; Tatsumi, K.; Fujieda, T.; Prosini, P. P.; Sakai, T. *J. Electrochem. Soc.* **2000**, *147*, 2050−2056.
(17) Kobayashi, Y.; Miyashiro, H.; Seki, S.; Yamanaka, A.; Mita, Y.; Iwahori, T. *CRIEPI Report* **2005**, Q04001 in Japanese.
(18) Kobayashi, T.; Shono, K.; Tabuchi, M.; Kobayashi, Y.; Miyashiro, H. *CRIEPI Report* **2012**, Q11020 in Japanese.
(19) Li, J.; Klöpsch, R.; Nowak, S.; Kunze, M.; Winter, M.; Passerini, S. *J. Power Sources* **2011**, *196*, 7687−7691.
(20) Guerfi, A.; Kaneko, M.; Petitclerc, M.; Mori, M.; Zaghib, K. *J. Power Sources* **2007**, *163*, 1047−1052.
(21) Kobayashi, Y.; Seki, S.; Mita, Y.; Ohno, Y.; Miyashiro, H.; Charest, P.; Guerfi, A.; Zaghib, K. *J. Power Sources* **2008**, *185*, 542−548.
(22) Yabuuchi, N.; Ohzuku, T. *J. Power Sources* **2005**, *146*, 636−639.
(23) Ohzuku, T.; Makimura, Y. *Chem. Lett.* **2001**, *30*, 642−643.
(24) Kobayashi, Y.; Kihira, N.; Takei, K.; Miyashiro, H.; Kumai, K.; Terada, N.; Ishikawa, R. *J. Power Sources* **1999**, *81−82*, 463−466.
(25) Reale, P.; Privitera, D.; Panero, S.; Scrosati, B. *Solid State Ionics* **2007**, *178*, 1390−1397.
(26) Liu, S.; Imanishi, N.; Zhang, T.; Hirano, A.; Takeda, Y.; Yamamoto, O.; Yang, J. *J. Power Sources* **2010**, *195*, 6847−6853.
(27) Appetecchi, G. B.; Croce, F.; Dautzenberg, G.; Mastragostino, M.; Ronci, F.; Scrosati, B.; Soavi, F.; Zanelli, A.; Alessandrini, F.; Prosini, P. P. *J. Electrochem. Soc.* **1998**, *145*, 4126−4132.
(28) Han, H.-B.; Zhou, S.-S.; Zhang, D.-J.; Feng, S.-W.; Li, L.-F.; Liu, K.; Feng, W.-F.; Nie, J.; Li, H.; Huang, X.-J.; Armand, M.; Zhou, Z.-B. *J. Power Sources* **2011**, *196*, 3623−3632.
(29) Gabrisch, H.; Yi, T.; Yazami, R. *Electrochem. Solid-State Lett.* **2008**, *11*, A119−A124.
(30) Johan, M. R.; Shy, O. H.; Ibrahim, S.; Mohd Yassin, S. M.; Hui, T. Y. *Solid State Ionics* **2011**, *196*, 41−47.
(31) Ismiyev, A. M.; Maharramov, A. M.; Aliyeva, R. A.; Askerov, R. K.; Mahmudov, K. T.; Kopylovich, M. N.; Naïli, H.; Pombeiro, A. J. L. *J. Mol. Struct.* **2013**, *1032*, 83−87.